RTFF: Random-to-Target Fabric Flattening Policy using Dual-Arm Manipulator

Kai Tang^{1,2,†}, Dipankar Bhattacharya^{1,2,†}, Hang Xu², Fuyuki Tokuda^{1,2}, Norman C. Tien^{2,3}, and Kazuhiro Kosuge^{1,2}

Abstract—Robotic fabric manipulation in garment production for sewing, cutting, and ironing requires reliable flattening and alignment, yet remains challenging due to fabric deformability, effectively infinite degrees of freedom, and frequent occlusions from wrinkles, folds, and the manipulator's End-Effector (EE) and arm. To address these issues, this paper proposes the first Random-to-Target Fabric Flattening (RTFF) policy, which aligns a random wrinkled fabric state to an arbitrary wrinkle-free target state. The proposed policy adopts a hybrid Imitation Learning-Visual Servoing (IL-VS) framework, where IL learns with explicit fabric models for coarse alignment of the wrinkled fabric toward a wrinkle-free state near the target, and VS ensures fine alignment to the target. Central to this framework is a template-based mesh that offers precise target state representation, wrinkle-aware geometry prediction, and consistent vertex correspondence across RTFF manipulation steps, enabling robust manipulation and seamless IL-VS switching. Leveraging the power of mesh, a novel IL solution for RTFF-Mesh Action Chunking Transformer (MACT)—is then proposed by conditioning the mesh information into a Transformer-based policy. The RTFF policy is validated on a real dual-arm tele-operation system, showing zero-shot alignment to different targets, high accuracy, and strong generalization across fabrics and scales. Project website: https://kaitang98.github.io/RTFF_Policy/

I. INTRODUCTION

Robotic manipulation of fabrics is a promising approach to reduce labor and enhance efficiency in garment production. A key task is sewing, where the same fabric must be reloaded in different positions to stitch seams such as the shoulder and sides of a T-shirt, and random wrinkles are inherently introduced during sewing, loading and repositioning. [1] To ensure accurate seam placement, fabric needs to be manipulated from such *initial random wrinkled states* to a wrinkle-free, flattened target state, whose pose (orientation and translation) varies across processes. This task, referred to as Random-to-Target Fabric Flattening (RTFF) (Fig. 1), typically requires iterative selecting grasping points, flattening, adjusting pose, and aligning until the target state

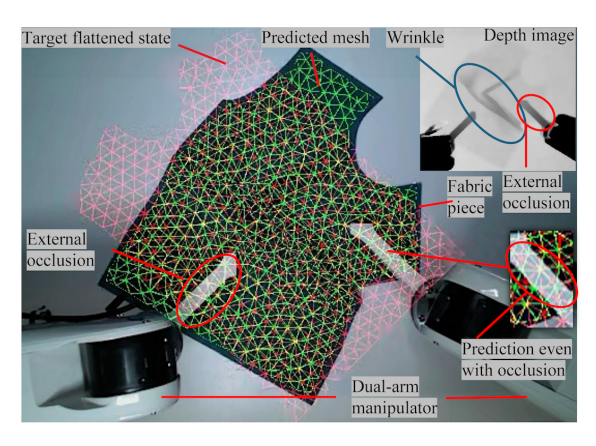


Fig. 1: Random-to-Target Fabric Flattening (RTFF) task.

is reached [2]. Efficient RTFF is also equally critical in fabric cutting, screen printing, and ironing, where flatness and precise alignment determine garment quality [1], [3].

While RTFF is essential in garment production, most classical alignment methods are designed for rigid objects using *Visual Servoing (VS)*, which reduces error between the observed and target states by calculating the *inverse Jacobian* that maps error changes to robot motions in real time [4]. However, in RTFF the fabric's deformability yields complex, non-linear deformations and effectively infinite Degrees of Freedom (DoF) [5], making the task underactuated with limited manipulator DoF, complicating *grasping points* selection and inverse Jacobian estimation [6].

Recently, *Imitation Learning (IL)* has become popular for fabric manipulation such as flattening [7] and folding [8]. By learning the observation-action mapping directly from expert demonstrations, IL eliminates the need for explicit models of fabric deformability and dynamics. Thus, IL demonstrates promising potential in RTFF, for example, transforming a wrinkled fabric to a wrinkle-free state, enabling coarse alignment, and providing demonstration-informed grasping points to VS. However, IL faces two key challenges in RTFF: i) most existing IL approaches [8]–[11] generate a sequence of actions (referred to as an action chunk), by directly conditioned on RGB or RGB-D images, which limits the ability of IL policies to specify various targets, identify robust wrinkle features from fabric images and to track alignment errors between the fabric current and target state; ii) achieving both high-precision manipulation and generalization across diverse wrinkled fabric and target states typically requires large, costly datasets of expert demonstrations [10].

Consequently, a natural direction is a hybrid IL-VS policy

[†]These authors contributed equally to this work.

¹K. Tang, D. Bhattacharya, F. Tokuda and K. Kosuge are with the JC STEM Lab of Robotics for Soft Materials, Department of Electrical and Electronic Engineering, Faculty of Engineering, The University of Hong Kong, Hong Kong SAR, China, (e-mail: tangkai@eee.hku.hk; kosuge@hku.hk).

²K. Tang, D. Bhattacharya, H. Xu, F. Tokuda, N. C. Tien, and K. Kosuge are with the Centre for Transformative Garment Production, 12/F, Building 19W, Hong Kong Science Park, Hong Kong SAR, China, (e-mail: d.bhattacharya@transgp.hk; hang.xu@transgp.hk; fuyuki.tokuda@transgp.hk).

³N. C. Tien is with the Department of Electrical and Electronic Engineering, Faculty of Engineering, The University of Hong Kong, Hong Kong SAR, China, (e-mail: nctien@hku.hk).

that leverages the strengths of both paradigms for RTFF: IL is first used to flatten the initially wrinkled fabric and obtain *coarse alignment*, followed by VS to achieve *fine alignment*. The primary challenge in realizing this integration is accurate and efficient fabric *state estimation*, since both paradigms require a consistent geometric representation of the fabric for precise RTFF problem formulation and fabric manipulation and alignment, which is the key bridge to a unified RTFF policy. However, fabric state estimation is challenging due to fabric's effectively infinite DoF. Additionally, *self-occlusions* from wrinkles and folds and *external-occlusions* from the manipulator's End-Effector (EE) and arm during RTFF, obscure fabric perception and thereby limit state estimation.

State estimation can be achieved with the template mesh method, where a mesh represents fabric as a grid of vertices connected by edges, and a canonical template mesh serves as an undeformed reference that can be deformed into various fabric states, while preserving vertex correspondences [12]. This approach offers several benefits: (i) the predicted mesh encodes wrinkle information such as location, depth, and shape, enabling wrinkle-aware reasoning, supporting IL in proposing grasping points, and guiding manipulation toward the target; (ii) the target state can be precisely specified using template mesh, enabling alignment error tracking—a prerequisite for applying IL in RTFF—and facilitating natural IL-VS switching by computing alignment error magnitude and fabric flatness; (iii) the correspondence-preserving template ensures consistent vertex mapping between simulated and real fabric states, as well as across predicted deformation states at successful time steps, thereby enabling direct simto-real transfer and accurate deformation tracking; and (iv) the predicted mesh accounts for both self- and external occlusions, which is essential for RTFF policy design.

Hence, this work proposes a novel RTFF policy to select grasping points and actions that reduce fabric wrinkles, adjust pose, and progressively align the fabric mesh to the target. The contributions of this paper are as follows:

- To the best of the authors' knowledge, this work is the first to introduce an Random-to-Target Fabric Flattening (RTFF) policy by integrating template mesh-based state estimation with a hybrid IL-VS framework.
- The template-based mesh representation of fabric allows precise target state definitions, wrinkle shape awareness, correspondence-preserving inputs for robotic fabric manipulation, and seamless switching between IL and VS.
- As a novel IL solution, Mesh Action Chunking Transformer (MACT) incorporates template-based mesh fabric representation into a Transformer-based policy, achieving robust and generalized fabric alignment via a reduced set of demonstrations.
- The proposed RTFF policy is validated via physical experiments on a real dual-arm tele-operation system, demonstrating zero-shot alignment, high accuracy, and strong generalization across fabrics.

II. RELATED WORK

State estimation: Fabric state estimation has been extensively studied using pixels [6], [13], edges [14], latent vectors [15], point clouds [16], and meshes [17], [18], but these methods lack correspondence-preserving representations for consistent mapping across different deformation states of the same fabric, and hinder sim-to-real transfer. By incorporating a template mesh [12] for state estimation, the proposed framework preserves correspondence and enforces geometric consistency across deformation states, while inferring both self- and externally-occluded fabric regions.

Learning-based fabric manipulation: Learning-based policies have recently advanced fabric manipulation tasks such as alignment [6], flattening [7], and folding [19]. Existing approaches either follow a model-based pipeline—first learning fabric dynamics and then performing planning and control [4]—or are trained end-to-end via reinforcement learning [20] or IL [8]-[10]. Among these, teleoperationbased IL avoids explicit dynamics modeling, complex objective design, and large sim-to-real gaps by directly learning expert strategies, making it well-suited for manipulation tasks. However, existing IL methods typically rely on RGB or RGB-D inputs and require large demonstration datasets, limiting alignment precision and accuracy in RTFF and their learning efficiency [8]–[11]. In contrast, the proposed MACT encodes fabric features explicitly into a mesh and additionally incorporates real-time alignment error as policy inputs. This design achieves precise alignment and generalization across diverse target states in RTFF, while requiring only a small number of demonstrations.

Visual Servoing: Fabric manipulation with VS has been widely explored. For wrinkle-free states, prior methods align fabric to targets by assuming near-rigid behavior [4], [21] or by tensioning the fabric using a dual-arm manipulator to approximate rigid-body motion [1], [6], [13]. These assumptions break down with large initial misalignment with the target state, where VS fails [1], [6]. The proposed framework addresses these challenges by estimating a correspondence-preserving fabric mesh that guides IL toward the target mesh, producing a feasible initialization and demonstration-informed grasping points to VS.

III. PROPOSED FRAMEWORK OUTLINE

This section outlines the robotic platform, formulates the RTFF task, and introduces fabric state estimation and RTFF manipulation policy.

A. Robotic manipulation platform

The robotic manipulation platform (Fig. 2 (b)) consists of two 6-DoF manipulators suspended from an aluminum frame, each with a wrist-mounted F/T sensor and a custom end-effector. Dual-arm impedance control [1] enables safe interaction with the environment without joint torque sensing. An RGB-D sensor on top provides images for real-time state estimation. Human demonstration data for RTFF is collected via teleoperation using two SpaceMouse devices to command end-effector velocities and desired forces. A

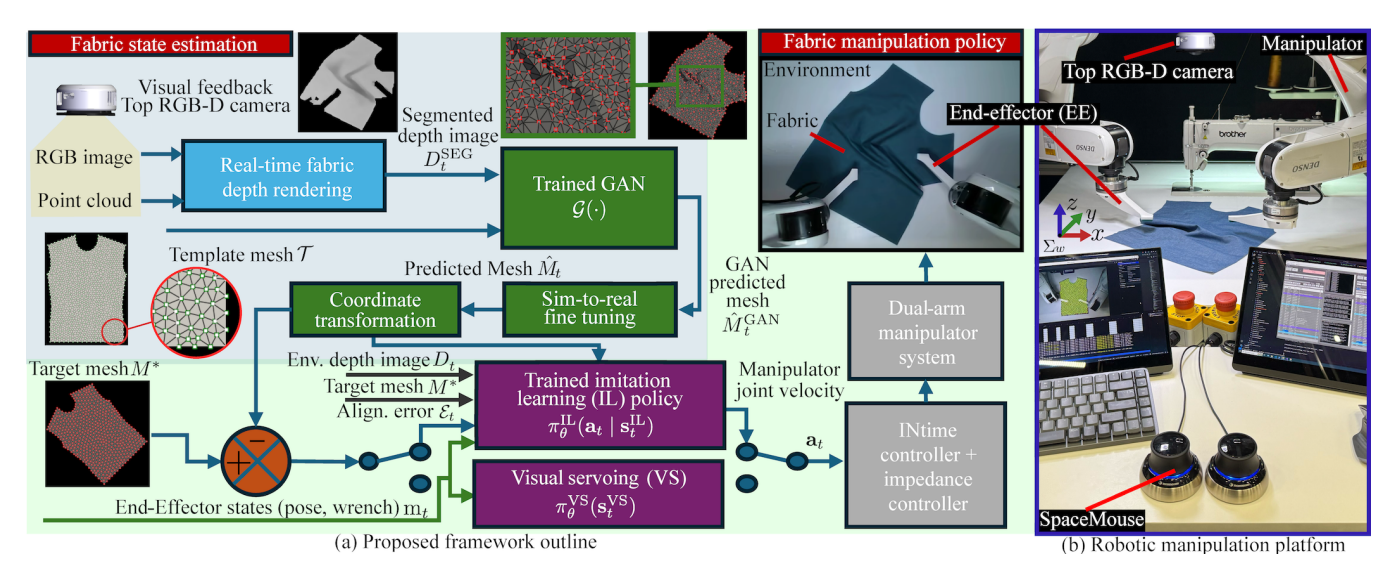


Fig. 2: Overview of the proposed RTFF policy framework.

low-level workstation provides high-frequency control of the manipulators, while a high-level computer runs state estimation and RTFF policy modules at a lower frequency.

For operating the platform, a world frame $\Sigma_{\mathbf{w}}$ (Fig. 2 (b)) is defined with the z-axis normal to the table and all vectors are expressed in this frame. At time t, the proprioceptive state of end-effector $i \in \{L,R\}$ (L left, R right) is $\mathbf{m}_{t,i} \in \mathbb{R}^{12}$, containing its 6D pose and wrench; the combined state is $\mathbf{m}_t = [\mathbf{m}_{t,L}^\top, \mathbf{m}_{t,R}^\top]^\top \in \mathbb{R}^{24}$. The action of the manipulator i is $\mathbf{a}_{t,i} = [v_{x,i}, v_{y,i}, \omega_{z,i}, F_{z,i}^d]^\top$, with $v_{x,i}, v_{y,i}$ planar velocities, $\omega_{z,i}$ yaw rate, and $F_{z,i}^d$ the desired vertical force for impedance control. The joint action $\mathbf{a}_t = [\mathbf{a}_{t,L}^\top, \mathbf{a}_{t,R}^\top]^\top \in \mathbb{R}^8$ drives the end-effectors for fabric manipulation.

B. RTFF task description

Let the canonical template mesh be $\mathcal{T}=(V^{\text{TPL}},E^{\text{TPL}})$, a standardized flattened fabric reference derived from the fabric CAD model. Here, $V^{\text{TPL}}=\{\mathbf{v}_i^{\text{TPL}}\}_{i=1}^N$ are vertex positions, and $E^{\text{TPL}}\subseteq\{(i,j)\mid i\neq j\}, |E^{\text{TPL}}|=N_e,$ are triangular mesh that connects the vertices. At time t, the RGB-D input and \mathcal{T} are used for state estimation to predict the deformed mesh $\hat{M}_t=(\hat{V}_t,E^{\text{TPL}})$, with $\hat{V}_t=\{\hat{\mathbf{v}}_{i,t}\}_{i=1}^N$. Reusing E^{TPL} preserves vertex connectivity. Given a wrinkle-free, flattened target mesh derived from the template mesh (red, Fig. 1), $M^*=(V^*,E^{\text{TPL}})$, with $V^*=\{\mathbf{v}_i^*\}_{i=1}^N$, the mean alignment error between the predicted mesh \hat{M}_t and the target mesh M^* at time t along x,y,z is

$$\bar{\mathbf{e}}_t = \frac{1}{N} \sum_{i=1}^{N} \mathbf{e}_{i,t}, \quad \text{where} \quad \mathbf{e}_{i,t} = \hat{\mathbf{v}}_{i,t} - \mathbf{v}_i^* \in \mathbb{R}^3.$$
 (1)

Here, $\bar{\mathbf{e}}_t \in \mathbb{R}^3$, and $\mathbf{e}_{i,t}$ denotes the i^{th} vertex alignment error. The template mesh \mathcal{T} , shared by \hat{M}_t and M^* , ensures correspondence-preserving state estimation, deformation tracking, and sim-to-real transfer. **Note:** Throughout the paper, M (such as M^*, \hat{M}) denotes the vertex position V (such as V^*, \hat{V}), by slight abuse of notation, although it formally represents the mesh (V, E^{TPL}) .

Definition 1 (RTFF task): Assuming fabric wrinkles do

not involve irreversible deformations (such as stretched fibers or permanent creases) and that the fabric can be fully flattened on the table with a sufficient sequence of dual-arm actions $\mathbf{a}_{0:T-1} = \{\mathbf{a}_0, \dots, \mathbf{a}_{T-1}\}$, the RTFF task is formulated as minimizing the terminal mean alignment magnitude (terminal mean alignment norm) over $\mathbf{a}_{0:T-1}$

$$\min_{\mathbf{a}_{0:T-1}} \|\bar{\mathbf{e}}_T(M_T, M^*)\|_2, \tag{2}$$

where T denotes the planning horizon. Equation (2) evaluates the final state after $\mathbf{a}_{0:T-1}$ transforms the initial wrinkled mesh \hat{M}_0 into M^* .

C. RTFF policy

The key challenge in RTFF is wrinkled fabric state estimation under occluded RGB-D, while tracking mesh states to plan manipulator actions. This section first introduces state estimation to handle occlusions, followed by the policy.

1) Fabric state estimation: The fabric state estimation of RTFF policy predicts the fabric mesh (green, Fig. 1). The current RGB image and point cloud are first processed by a fabric depth rendering module to produce segmented point cloud $Q_t^{\rm SEG}$, and segmented fabric depth image $D_t^{\rm SEG}$ at time t. Next, $D_t^{\rm SEG}$ and \mathcal{T} are input to a Graph Attention Network (GAN), $\mathcal{G}(\cdot)$, trained on synthetic data from a triangular mass-spring mesh model with occlusions, to predict the deformed fabric mesh $\hat{M}_t^{\rm GAN}$ in real time. However, to ensure smoother mesh-prediction transitions between consecutive time steps of the manipulation policy, and further improve accuracy, sim-to-real fine-tuning is performed, in which $\hat{M}_t^{\rm GAN}$ is refined by a residual correction $\delta \hat{M}\left(\hat{M}^{\rm GAN}, Q^{\rm SEG}\right)$ by optimizing a one-sided Chamfer loss that aligns the mesh with $Q^{\rm SEG}$. The final prediction can be written as

$$\hat{M}_t = \hat{M}_t^{\text{GAN}} + \delta \hat{M}_t(\cdot), \text{ with } \hat{M}_t^{\text{GAN}} = \mathcal{G}(D_t^{\text{SEG}}, \mathcal{T}).$$
 (3)

2) Fabric manipulation policy: Given the prediction from (3), fabric manipulation is formulated as a Markov Decision Process (MDP) $\mathcal{M} = (\mathcal{S}, \mathcal{A}, \mathcal{P})$, where the observation state at time t is $\mathbf{s}_t = \{M^*, \hat{M}_t, D_t, \mathcal{E}_t, \mathbf{m}_t\} \in \mathcal{S}$, where D_t

the environment depth image and alignment error $\mathcal{E}_t = \{\mathbf{e}_{i,t}\}_{i=1}^N$. Given \mathbf{s}_t and action $\mathbf{a}_t \in \mathcal{A}$, transition $\mathcal{P}(\mathbf{s}_{t+1} \mid \mathbf{s}_t, \mathbf{a}_t)$ captures nonlinear fabric dynamics.

To solve the RTFF task, a hybrid manipulation policy $\pi_{\theta}: \mathcal{S} \to \mathcal{A}$ is proposed, consisting of an IL policy $\pi_{\theta}^{\mathrm{IL}}$ for coarse alignment and a VS policy $\pi_{\theta}^{\mathrm{VS}}$ for fine alignment. Given state $\mathbf{s}_t^{\mathrm{IL}} = \mathbf{s}_t$, the IL policy is modeled as the conditional distribution $\pi_{\theta}^{\mathrm{IL}}(\mathbf{a}_t \mid \mathbf{s}_t^{\mathrm{IL}})$, which is fit implicitly from human demonstrations. The learned policy generates sequence of manipulation actions \mathbf{a}_t such as grasp point selection, fabric flattening, pose adjustment, and coarse alignment to M^* . For the VS policy, the reduced state $\mathbf{s}_t^{\mathrm{VS}} = \{M^*, \hat{M}_t, \mathcal{E}_t, \mathbf{m}_t\}$ is used to design a closed-loop control law $\pi_{\theta}^{\mathrm{VS}}(\mathbf{s}_t^{\mathrm{VS}})$ which coordinates dual-arm actions for fine alignment. Note that \mathcal{P} is implicit in IL (learned from demonstrations) and explicit in VS (defined by interaction Jacobian).

Definition 2 (RTFF policy): The hybrid policy is given by

$$\mathbf{a}_{t} \sim \begin{cases} \pi_{\theta}^{\text{IL}}, & \text{if } \Phi_{t} < \epsilon_{\Phi}, \ \|\bar{\mathbf{e}}_{t}\|_{2} > \epsilon_{\bar{\mathbf{e}}}, \ F_{z,i,t} < F_{z}^{g}, \\ \pi_{\theta}^{\text{VS}}, & \text{if } \Phi_{t} \geq \epsilon_{\Phi}, \ \|\bar{\mathbf{e}}_{t}\|_{2} \leq \epsilon_{\bar{\mathbf{e}}}, \ F_{z,i,t} \geq F_{z}^{g}, \end{cases}$$
(4)

where $\Phi_t \in [0,1]$ is flatness, the fraction of mesh vertices on tabletop within a height tolerance; $\|\bar{\mathbf{e}}_t\|_2$ is the alignment error magnitude (mean alignment error norm); and $F_{z,i,t}$ is the EE vertical force with $i \in \{L,R\}$. The IL policy first performs coarse alignment to reduce wrinkles and bring the fabric closer M^* . When the fabric is flat and aligned, $\Phi_t \geq \epsilon_{\Phi}$ and $\|\bar{\mathbf{e}}_t\|_2 \leq \epsilon_{\bar{\mathbf{e}}}$, IL selects grasping points for handoff. After both arms grasp the fabric, $F_{z,i,t} \geq F_z^g$, control switches to π_{θ}^{VS} for fine alignment, producing the action sequence $\mathbf{a}_{0:T-1}$ that minimizes (2).

3) MACT: This work implements IL with a novel MACT policy that conditions on the predicted mesh \hat{M} from (3), the target mesh M^* , and the alignment error \mathcal{E}_t using a Transformer backbone. The policy outputs action chunks [9] for efficient storage and execution while capturing non-Markovian behaviors in demonstrations. Given an observation $\mathbf{s}_t^{\mathrm{IL}}$, MACT predicts a horizon of N_h actions $\hat{\mathbf{a}}_{t:t+N_h}$. Hence the one-step IL policy $\pi_{\theta}^{\mathrm{IL}}(\mathbf{a}_t \mid \mathbf{s}_t^{\mathrm{IL}})$ in (4) can be extended and re-written as $\pi_{\theta}^{\mathrm{IL}}(\hat{\mathbf{a}}_{t:t+N_h} \mid \mathbf{s}_t^{\mathrm{IL}})$. At deployment, this horizon is executed in a receding manner via temporal ensembling—overlapping predictions are averaged to yield the next action, thereby recovering $\pi_{\theta}^{\mathrm{IL}}(\mathbf{a}_t \mid \mathbf{s}_t^{\mathrm{IL}})$. Finally, MACT supervision is provided by a reconstruction loss, computed as the ℓ_1 discrepancy between $\hat{\mathbf{a}}_{t:t+N_h}$ and the ground-truth chunk $\mathbf{a}_{t:t+N_h}$ from demonstrations, averaged across N_h .

IV. METHODOLOGY

This section presents implementation of RTFF policy.

A. State estimation implementation

1) Synthetic data generation: A fabric state is modeled as a triangular mass–spring mesh $M^{\rm SIM}=(V^{\rm SIM},E^{\rm TPL}),$ where $V^{\rm SIM}=\{{\bf v}_i^{\rm SIM}\}_{i=1}^N$ are 3D vertex positions and $E^{\rm TPL}$ connects neighboring vertices as point masses. Each edge $(i,j)\in E^{\rm TPL}$ acts as a spring with vector ${\bf d}_{ij}^{\rm SIM}={\bf v}_j^{\rm SIM}-{\bf v}_i^{\rm SIM},\quad \|{\bf d}_{ij}^{\rm SIM}\|_2,$ enforcing structural constraints. This mesh is implemented in

Blender [22]. To generate diverse states, randomized manipulations were applied, including multi-hand and single-hand interactions (with or without lifting), as well as compression and shearing. After each manipulation, the final deformed mesh $M^{\rm SIM}$ is saved as the simulation output.

After mesh generation, depth images are rendered with Py-Torch3D [23]. Centralized meshes are batched and processed with a custom depth shader, normalizing z-buffer values to a fixed range. The outputs are converted to single-channel grayscale depth images, and the resulting $D^{\rm SIM}$ from $M^{\rm SIM}$ are saved for training the GAN in fabric state estimation. Finally, each depth image $D^{\rm SIM}$ is converted to a simulated point cloud $Q^{\rm SIM} = \{ {\bf q}_j^{\rm SIM} \in \mathbb{R}^3 \mid j=1,\dots,N_q^{\rm SIM} \}$, by mapping each pixel to a 3D point.

2) Mesh prediction model: The mesh prediction model follows a GAN framework composed of three components, described as follows.

Input encoding: The mesh prediction model employs a GAN-based encoder integrating image features and template graph encodings. A ResNet backbone encodes the depth image D^{SIM} into feature f, which together with the template mesh $\mathcal{T} = (V^{\text{TPL}}, E^{\text{TPL}})$ forms the initial template graph $\bar{G}^{(0)} = (\bar{V}^{(0)}, \bar{E}^{(0)})$, with vertex features $\bar{V}^{(0)} = \{\bar{v}_i^{(0)}\}_{i=1}^N$ and edge features $\bar{E}^{(0)} = \{\bar{e}_{ij}^{(0)}\}_{i,j=1}^N$. The initial encodings are $\bar{v}_i^{(0)} = \text{MLP}_V([\mathbf{v}_i^{\text{TPL}}, f])$ and $\bar{e}_{ij}^{(0)} = \text{MLP}_E([\mathbf{d}_{ij}^{\text{TPL}}, \|\mathbf{d}_{ij}^{\text{TPL}}\|_2])$, where $\mathbf{d}_{ij}^{\text{TPL}} = \mathbf{v}_i^{\text{TPL}} - \mathbf{v}_j^{\text{TPL}}$. Graph attention updating: In the baseline GNN, vertex $\bar{v}_i^{(l)}$ and edge $\bar{e}_{ij}^{(l)}$ features are updated by averaging paighbors, with $l \in \{0, \dots, L-1\}$ denoting the layer

Graph attention updating: In the baseline GNN, vertex $\bar{v}_i^{(l)}$ and edge $\bar{e}_{ij}^{(l)}$ features are updated by averaging neighbors, with $l \in \{0,\dots,L-1\}$ denoting the layer index. To enhance message passing, an attention mechanism from GAT [24] is adopted, pooling neighboring edges with learnable weights, and the updates follow [12].

Fabric Mesh Decoding: After L graph updates, each vertex feature $\bar{v}_i^{(L)}$ is decoded into a predicted position $\hat{\mathbf{v}}_i^{\mathrm{GAN}} \in \mathbb{R}^3$, supervised by a synthetic dataset. The decoding process can be written as $\mathrm{MLP}_D([\bar{v}_i^{(L)}])$.

Training Loss: The template-based GAN $\mathcal{G}(\cdot)$ is supervised on synthetic datasets (Sec. IV-A.1). The objective is

$$\mathcal{L}_{\text{GAN-Train}} = \mathcal{L}_{\text{Vtx}} + \lambda_k \mathcal{L}_{\text{Kev}} + \lambda_c \mathcal{L}_{\text{Cham}}.$$
 (5)

The vertex loss measures ℓ_1 distance between predicted vertices $\hat{\mathbf{v}}_i^{\text{GAN}}$ and ground truth $\mathbf{v}_i^{\text{SIM}}$, while the keypoint loss applies the same penalty on semantic keypoints (neckline, shoulder, arm, hem):

$$\mathcal{L}_{\text{Vtx}} = \frac{1}{N} \sum_{i=1}^{N} ||\Delta \mathbf{v}_i||_1, \ \mathcal{L}_{\text{Key}} = \frac{1}{N_k} \sum_{i \in \text{Key}} ||\Delta \mathbf{v}_i||_1, \ (6)$$

where $\Delta \mathbf{v}_i = \hat{\mathbf{v}}_i^{\text{GAN}} - \mathbf{v}_i^{\text{SIM}}$, N_k denotes number of keypoints. To refine boundary and surface similarity, the Chamfer loss measures distances from the simulated point cloud Q^{SIM} to predicted vertices

$$\mathcal{L}_{\text{Cham}} = \frac{1}{N^{\text{SIM}}} \sum_{\mathbf{q}_{i}^{\text{SIM}} \in Q^{\text{SIM}}} \min_{\hat{\mathbf{v}}_{i}^{\text{GAN}}} \|\hat{\mathbf{v}}_{i}^{\text{GAN}} - \mathbf{q}_{j}^{\text{SIM}}\|_{2}. \quad (7)$$

Finally, $\mathcal{G}(\cdot)$ is trained by minimizing (5) with meshes M^{SIM} as ground truth and depth images D^{SIM} as input.

3) Real Fabric Depth Rendering: At time t, the segmented depth image $D_t^{\rm SEG}$ is produced by a GPU-accelerated

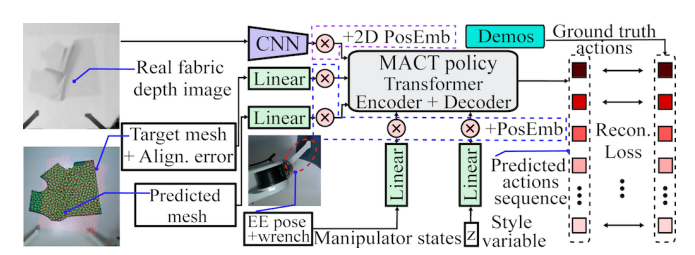


Fig. 3: MACT policy architecture.

pipeline. RGB and point cloud data are first captured with the Realsense sensor (Sec. III-A). SAM2 [25] segments the RGB frame to obtain a fabric mask, which is applied to the point cloud using Torch functions to isolate fabric points. The resulting cloud is denoised and centralized, yielding $Q_t^{\rm SEG} = \{ \mathbf{q}_j^{\rm SEG} \in \mathbb{R}^3 \mid j=1,\ldots,N_q^{\rm SEG} \}, \text{ where } N_{q,t}^{\rm SEG} \text{ is the number of points. Finally, } Q_t^{\rm SEG} \text{ is rasterized with PyTorch3D to form } D_t^{\rm SEG} \text{ for fabric state estimation.}$

4) Sim-to-real fine tuning: To obtain the residual correction $\delta \hat{M}\left(\hat{M}^{\text{GAN}},Q^{\text{SEG}}\right)$ defined in Sec. III-C.1, a one-sided Chamfer loss that aligns the GAN predicted mesh \hat{M}^{GAN} with the segmented point cloud Q^{SEG} is written as

$$\mathcal{L}_{\text{Cham-R}} = \frac{1}{N_i^{\text{SEG}}} \sum_{\mathbf{q}_i^{\text{SEG}} \in Q^{\text{SEG}}} \min_{\hat{\mathbf{v}}_i^{\text{GAN}}} \|\hat{\mathbf{v}}_i^{\text{GAN}} - \mathbf{q}_j^{\text{SEG}}\|_2.$$
(8)

To avoid vertex drift, an edge-length regularization preserves local mesh structure is defined as

$$\mathcal{L}_{\text{Edge-R}} = \frac{1}{N_e} \sum_{(i,j) \in E^{\text{TPL}}} \left| \| \hat{\mathbf{d}}_{ij}^{\text{GAN}} \|_2 - \| \mathbf{d}_{ij}^{\text{TPL}} \|_2 \right|.$$
 (9)

The final objective is

$$\mathcal{L}_{R} = \lambda_{\text{Cham-R}} \, \mathcal{L}_{\text{Cham-R}} + \lambda_{\text{Edge-R}} \, \mathcal{L}_{\text{Edge-R}}, \tag{10}$$

where weights $\lambda_{\text{Cham-R}}$ and $\lambda_{\text{Edge-R}}$ balance alignment and regularity. Minimization of \mathcal{L}_{R} provides the residual correction $\delta \hat{M}$ to the GAN prediction, defined as $\delta \hat{M} = \arg\min_{\Delta M} \ \mathcal{L}_{\text{R}} \Big(\hat{M}^{\text{GAN}} + \Delta M, Q^{\text{SEG}} \Big)$, which yields the final predicted mesh (3).

B. Hybrid manipulation policy implementation

1) Mesh Action Chunking Transformer (MACT): The MACT policy (Sec. III-C.2, Fig. 3) takes as input a $D_t \in \mathbb{R}^{H \times W \times 1}$ depth image, which is encoded by a ResNet-18 backbone into a feature map of size $\mathbb{R}^{H' \times W' \times d_{\text{model}}}$, where d_{model} is a predefined model dimension. The feature is then flattened along the spatial dimension to obtain a $(H'W') \times d_{\text{model}}$ token sequence. To preserve spatial information, a 2D sinusoidal positional embedding is added to the feature sequence. Additional inputs include: (i) the target mesh \hat{V}^* with alignment error, $M^* \oplus \mathcal{E}_t \in \mathbb{R}^{N \times 6}$, embedded to $N \times d_{\text{model}}$; (ii) the predicted mesh vertices $\hat{V} \in \mathbb{R}^{N \times 3}$, embedded to $N \times d_{\text{model}}$; (iii) the EE states $\mathbf{m}_t = [\mathbf{m}_{t,L}^\top, \mathbf{m}_{t,R}^\top]^\top \in \mathbb{R}^{1 \times 24}$ (i.e., 2 manipulator, each with 6D position + 6D wrench), embedded to $1 \times d_{\text{model}}$. Additional sinusoidal positional embedding is added to these input sequences.

A style variable $z \in \mathbb{R}^{1 \times 24}$ is output by transformer-based Conditional Variational Autoencoder (CVAE). It takes as input the EE states and a target action sequence of length N_h prepended with a learned "[CLS]" token, forming a

 (N_h+2) sequence. The "[CLS]" feature outputs the mean and variance of z, which is sampled for training and set to the prior mean (zero) at inference for deterministic decoding. z is projected to $1\times d_{\mathrm{model}}$ via linear layers, yielding the concatenated encoder input $\mathbf{s}_t^{\mathrm{IL}}\in\mathbb{R}^{(H'W'+2N+2)\times d_{\mathrm{model}}}$.

The MACT decoder attends to encoder features via cross-attention, using a fixed $N_h \times d_{\text{model}}$ positional sequence as input. It outputs a $N_h \times d_{\text{model}}$ sequence, down-projected by an MLP to $N_h \times 8$, representing manipulator actions $\mathbf{a}_t = [\mathbf{a}_{t,L}^\top, \mathbf{a}_{t,R}^\top]^\top \in \mathbb{R}^8$ for the two manipulators over N_h steps. The model is trained with a VAE objective: reconstruction of action chunks plus a regularization term aligning the VAE encoder with a Gaussian prior.

2) Visual Servoing (VS): This section introduces the proposed position-based VS. At time t, the GAN-predicted mesh $\hat{M}_t = (\hat{V}_t, E^{\text{TPL}})$ meets the condition of π_{θ}^{VS} in (4). Assuming the fabric undergoes a rigid-body motion under dual-arm control [6], the mean alignment error between \hat{M}_t and the target mesh $M^* = (V^*, E^{\text{TPL}})$ given by (1) are reformulated as an objective function

$$\min_{R_t \in SO(3), \mathbf{t} \in \mathbb{R}^3} \frac{1}{N} \sum_{i=1}^{N} \left\| (R_t \hat{\mathbf{v}}_{i,t} + \mathbf{t}_t) - \mathbf{v}_i^* \right\|^2,$$
 (11)

where $\hat{\mathbf{v}}_{i,t} \in \hat{V}_t$, $\mathbf{v}_i^* \in V^*$ are corresponding vertices, and $T_t = (R, \mathbf{t}) \in SE(3)$ is the rigid-body transformation matrix w.r.t. $\Sigma_{\mathbf{w}}$. Since motion is restricted to the tabletop, T_t reduces to planar translation $\mathbf{p}_t = [x_t, y_t]^\top$ and rotation $\theta_t = \mathrm{atan2}(R_t(2, 1), R_t(1, 1))$. The pose error vector is then $\mathbf{\bar{e}}_t^p = (\mathbf{p}_t^\top, \theta_t)$, where the \mathbf{p}_t is the residual translation, and θ_t is the rotation to align \hat{M}_t with M^* .

To eliminate this $\overline{\mathbf{e}}_t^{\overline{p}}$, a coordinated motion of the dual-arm manipulator is calculated by introducing position-based VS and rigid body motion. The control motion is a planar spatial twist, $\mathbf{a}_t^{vs} = [v_x, v_y, \omega_z]^{\top} \subset \mathbf{a}_t$, defined in Sec. III-A, and F_z^d is set as a constant. In position-based VS, the error dynamics are written as

$$\dot{\bar{\mathbf{e}}}_t^p = L \, \mathbf{a}_t^{vs},\tag{12}$$

where L is the interaction matrix (Jacobian) by assuming a rigid body motion at time t. By imposing exponential decay of the error as $\dot{\bar{\mathbf{e}}}^p = -\lambda \bar{\mathbf{e}}^p$ with a gain $\lambda \in \mathbb{R}$, the control input can be expressed as

$$\mathbf{a}_{t}^{vs} = L^{\dagger} \dot{\mathbf{e}}_{t}^{p} = -\lambda L^{\dagger} \mathbf{\bar{e}}_{t}^{p}, \tag{13}$$

where L^{\dagger} is the Moore–Penrose pseudo-inverse of L. The control input is calculated at each iteration, providing real-time feedback that mitigates the impact of rigid-body assumptions and increases alignment precision [21].

3) Impedance control: Dual-arm impedance control is implemented to ensure the safety of interactions between the industrial manipulators and the environment [1], as well as regulates both internal fabric tension and external interaction forces, allowing for smooth adjustment toward the target mesh while preventing wrinkles and overstretching.

V. EXPERIMENTAL RESULTS

This section presents the hardware setup, state estimation results, and policy evaluations—including ablation on key

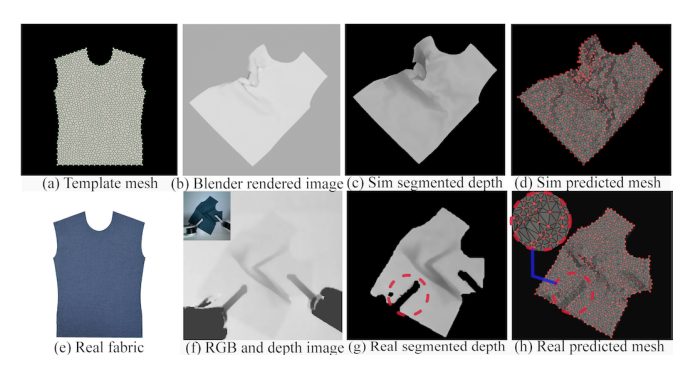


Fig. 4: Simulated and real fabric mesh prediction.

RTFF components and MACT, and generalization studies—to validate the RTFF policy framework, assuming wrinkles are reversible and the fabric can be flattened with sufficient dual-arm actions.

A. Hardware description

The manipulators in the proposed platform (Fig. 2 (b)) are DENSO VS-068 arms, each with an ATI Axia80-M8 F/T sensor and a custom 3D-printed end-effector. Teleoperation uses two SpaceMouse® Compact devices. The vision system is an Intel® RealSenseTM LiDAR Camera L515. The lower-level workstation is powered by an Intel® Xeon® W-2295 CPU running INtime OS over EtherCAT at 4k Hz, and the high-level computer is equipped with an NVIDIA GeForce RTX 4090 GPU, an Intel® CoreTM i9-14900KF CPU, and 128 GB RAM running Ubuntu 24.04 at 20 Hz.

B. State estimation results

This section presents state estimation results on a *T-shirt front panel* fabric with dimensions 400×550 mm; Fig. 4 (e). The canonical template mesh \mathcal{T} , with N=562 vertices (Fig. 4 (a)), is generated in MeshLab [26].

Synthetic data generation: For synthetic data generation in Blender, fabric simulation parameters were manually tuned for real fabric behavior. Random perturbations are applied during data generation to account for uncertain fabric parameters and mitigate the sim-to-real gap. Rendered cloth example in Blender is shown in Fig.4 (b). Finally, to generate simulated segmented depth image Fig.4 (c) for GAN training, the simulated fabric meshes M_t are saved and processed through the same depth rendering pipeline (Sec. IV-A.3) as real data to ensure consistency (Fig. 4 (c)).

Training mesh prediction model: About 60,000 simulated depth—mesh pairs were generated, split into 80% training, 10% validation, and 10% testing to train the GAN (Sec. IV-A.2). Training used depth inputs of 512×512 , batch size 16, 500 epochs, and a learning rate of 1×10^{-4} . The loss weights in (5) were $\lambda_k = 1$ and $\lambda_c = 0.5$. Data augmentation included: (i) additive Gaussian noise to reduce sensor sensitivity; (ii) random rigid-body rotations for viewpoint invariance; (iii) synthetic occlusions of various shapes and sizes to mimic EE and manipulator (external) occlusions, improving robustness to partial observability; and (iv) pixel-level z-variations to capture wrinkles. First, mesh \hat{M}^{GAN} is predicted from segmented depth D^{SEG} using the

trained GAN $\mathcal{G}(\cdot)$. Next, to improve prediction accuracy, the one-sided Chamfer loss (8) is optimized in real time using *Adam optimizer* with $\lambda_{\text{Cham-R}} = 1$, $\lambda_{\text{Edge-R}} = 0.01$, learning rate 2×10^{-3} , and five steps per observation yielding the final predicted mesh \hat{M} .

Fabric state estimation is first demonstrated in simulation, where depth input (Fig. 4 (c)) is processed by the trained GAN with data augmentation to predict meshes that recover fabric structure (Fig. 4 (d)). In the real case, regions missing due to EE occlusion (Fig. 4 (f)–(g), red circle) are similarly completed using the same approach, with Chamfer loss optimization improving prediction accuracy (Fig. 4 (h)).

C. Manipulation policy results

This section demonstrates the performance of the proposed RTFF manipulation policy pipeline. The policy is built on the LeRobot framework [27] and trained with human demonstrations collected on the robotic platform discussed in Sec. III-A. In this platform, fabric placement and wrinkle formation are inherently stochastic, so identical states cannot be reproduced. Thus, RTFF policy must be observation-driven, learning to localize wrinkles, plan motions to flatten and rotate the fabric to the target, select grasping points before switching to VS by using the current and target mesh, and coordinate collision-free dual-arm actions.

The data collection and evaluation process on this platform proceeds as follows: (i) the dual-arm manipulator is initialized to a home pose, and a wrinkled fabric is placed on the table; (ii) a target state M^* is randomly generated within the camera's field of view; (iii) demonstrations are collected by manually controlling the manipulators with a SpaceMouse to perform RTFF across multiple episodes, restricted to a single fabric type with fixed material and scale; (iv) these demonstrations are used to train the MACT component of the RTFF policy; (v) the trained policy is executed on fabrics with previously unseen wrinkles, thickness, textures, materials, and scales to flatten them toward the target states; (vi) finally, the manipulator returns to the home pose and experimental results are recorded for evaluation.

1) Experimental protocol and evaluation metrics: For experiments, a pre-defined set of fabric states and targets was needed, but consistent wrinkle reproduction was infeasible. To ensure fair comparison, 20 target meshes M^* were pre-sampled and used in all trials. Initial states were generated by orienting the neckline at 0°, 90°, 180°, and 270°, each with five trials introducing random wrinkles, yielding 20 states matching the 20 targets. Experimental parameters were set to $\epsilon_{\bar{\mathbf{e}}}=0.05\,\mathrm{m},\,\epsilon_{\Phi}=0.95,\,\mathrm{and}\,F_z^g=2.5\,\mathrm{N}.$

The RTFF policy is evaluated using three metrics: (i) terminal alignment error magnitude (terminal mean alignment error norm) $\|\bar{\mathbf{e}}_T\|_2$, where $\bar{\mathbf{e}}_T$ is given by (1) at t=T; (ii) failure, defined as $\|\bar{\mathbf{e}}_T\|_2 > 0.05\,\mathrm{m}$; and (iii) Intersection over Union (IoU) between the final mesh and target mesh M^* , measuring geometric overlap

$$IoU = \frac{|\mathbf{A}_{final} \cap \mathbf{A}_{M^*}|}{|\mathbf{A}_{final} \cup \mathbf{A}_{M^*}|},$$
(14)

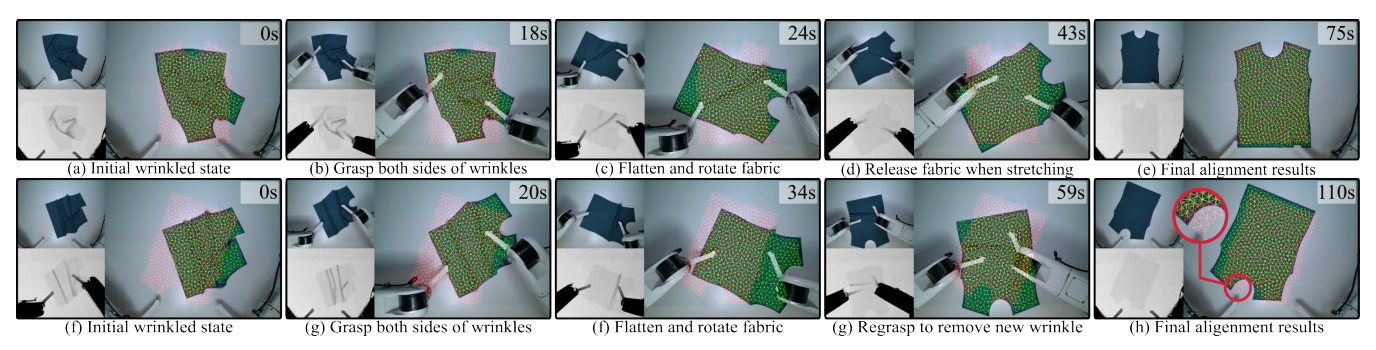


Fig. 5: Example RTFF sequences with (top) and without (bottom) Visual Servoing (VS).

where $\mathbf{A}_{\text{final}}$ and \mathbf{A}_{M^*} denote the final and target mesh regions. An IoU of 1 with sufficiently small $\|\mathbf{\bar{e}}_T\|_2$ indicates perfect alignment, while values near 0 imply negligible overlap. IoU is computed only for non-failure trials, and experiments terminate early if the first five trials all fail.

2) Human demonstrations and MACT training: Human demonstrations were used to train the IL component of the policy. In total, 50 episodes of 30–90 seconds each were collected at 20 Hz. To ensure a broad data distribution, random translations were applied to the fabric's initial position. For orientation coverage, the fabric's neckline is uniformly rotated on the table before wrinkles are introduced. To enhance robustness, online perturbations were introduced: (i) flattened regions of fabric were randomly re-wrinkled, and (ii) random displacements from the correct grasping point were applied by the operator through direct end-effector impedance control (without the SpaceMouse).

The MACT component of the RTFF policy was trained with depth inputs (640 \times 480), chunk size $N_h=100$, and model dimension $d_{\rm model}=512$. Training used 100,000 steps, a batch size of 4, and a learning rate of 1×10^{-5} .

3) RTFF policy evaluation: Table I, Row 1, reports the full RTFF policy, showing stable convergence to an average error of about 0.01 m after 20 trials with low variance, outperforming all ablations. During execution (Fig. 5, top

TABLE I: Ablation study of RTFF policy.

Method	Terminal alignment error magnitude (m)		IoU		Fail.
	Mean	Std.	Mean	Std.	ran.
Ours	0.011	0.002	0.926	0.018	-
w/o IL	-	-	-	-	5/5
w/o VS	0.028	0.010	0.871	0.05	-
w/o \hat{M}_t and \mathcal{E}_t	-	-	-	-	5/5
Туре	0.0145	0.004	0.911	0.031	-
Scale	0.021	0.004	0.893	0.022	-

row), the RTFF policy showed consistent behaviors: (i) adjusting the EE pose in the air and manipulating only after a successful grasp; (ii) grasping flat areas on both sides of wrinkles and removing them with opposing motions; (iii) releasing stretched fabric to restore shape before regrasping; (iv) smoothly switching to VS once criteria given by (4) is met; and (v) switching back to MACT if VS creates new wrinkles and voids (4), removing them before resuming VS. The results show that the policy achieves RTFF by learning fabric state and its relation to the target mesh. Using depth images with a mesh-based representation supports robust wrinkle extraction and accurate displacement

estimation between current and target states. With real-time visual feedback, the policy converges reliably across diverse initial configurations and unseen targets.

4) Ablation studies: Ablations were performed on key RTFF components and MACT: the IL policy, VS, \hat{M}_t , and \mathcal{E}_t . The ablation conditions are: (i) Without IL: Grasping points are still chosen by the trained IL policy for fairness, but execution proceeds with VS only. (ii) Without VS: The IL policy runs for up to 90 s per trial, after which the episode is terminated and outcomes recorded. (iii) Without current predicted fabric mesh \hat{M}_t and alignment error \mathcal{E}_t embeddings: Using the same data and hyperparameters, MACT (Fig. 3) was trained without \hat{M}_t and \mathcal{E}_t embeddings, retaining only the target mesh for RTFF.

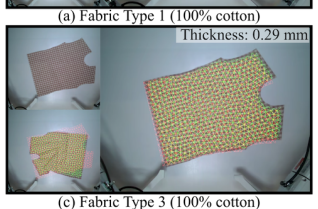
Ablation study results: Rows 2–4 of Table I report the results, with main findings: (i) Without IL: The policy failed, as VS alone cannot converge under nonlinear fabric deformations with infinite DoF, leading to uncontrollable dynamics. (ii) Without VS: The policy avoids outright failures but shows larger errors and variance, reflecting unreliability (Fig. 5, bottom row). Near the target, it fails to extract salient cues, leading to stationary behavior or repeated grasping at the same spot without moving the fabric. (iii) Without \hat{M}_t and \mathcal{E}_t embeddings: Training MACT with only environment depth image and the desired mesh embeddings also fails. Without explicit correspondence between current and target states, MACT cannot learn RTFF from limited demonstrations. While it sometimes flattens wrinkles, it cannot rotate or translate the fabric to match the target pose.

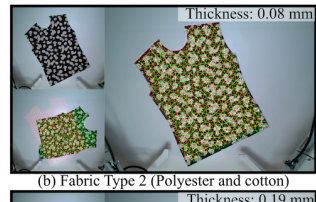
These results verify the central role of the mesh in the hybrid IL–VS policy. The mesh representation enables sample-efficient IL from few demonstrations, strengthens IL by providing a structured link between the current fabric state and the target, allowing for a smooth switching between IL and VS, and yields a well-defined representation that enables VS to converge \hat{M}_t to the given target.

5) Generalization experiments: In garment production, fabrics differ in color, material, and size. To test policy generalization, two additional experiments were conducted: (i) Type — five fabrics of different materials cut to the baseline shape, and (ii) Scale — the baseline fabric reduced to 80% size. Each experiment comprised 20 trials, with results given in Rows 5–6 of Table I and examples in Fig 6.

The results show that the policy successfully aligns unseen fabrics to desired target states. Depth images with predicted







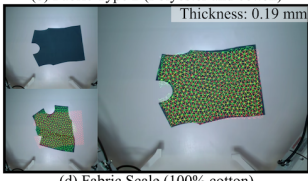


Fig. 6: Examples of various fabric Types(a)-(c) and Scale(d).

mesh enable robust wrinkle feature identification and accurate alignment error estimation between current and target states. Combined with real-time visual feedback, the policy converges across diverse fabric configurations, showing zero-shot generalization to various fabric types and sizes.

VI. CONCLUSION AND FUTURE WORK

This work presents the first Random-to-Target Fabric Flattening (RTFF) policy that integrates template mesh-based state estimation with a hybrid Imitation Learning-Visual Servoing (IL-VS) framework to align wrinkled fabric to diverse flattened targets. For state estimation under both self- and external occlusions, the template mesh provides an explicit representation that enables wrinkle-aware reasoning, supports IL in identifying grasp points, facilitates IL-VS switching, and ensures consistent mapping between various fabric deformation states. Incorporating this representation into a Transformer-based backbone yields Mesh Action Chunking Transformer (MACT), which is a novel IL policy with improved fabric manipulation ability and task generalization. Ablation studies highlight the central role of the mesh in the hybrid IL-VS policy, enabling zero-shot RTFF with fewer demonstrations and underscoring the framework's effectiveness. Future work focuses on extending the RTFF policy from planar, tabletop settings to full 3D manipulation.

ACKNOWLEDGMENT

This work was supported in part by the Innovation and Technology Commission of the HKSAR Government under the InnoHK initiative. The research described in this paper was conducted in part at the JC STEM Lab of Robotics for Soft Materials, funded by The Hong Kong Jockey Club Charities Trust.

REFERENCES

- [1] K. Tang, X. Huang, A. Seino, F. Tokuda, A. Kobayashi, N. C. Tien, and K. Kosuge, "Fixture-free automated sewing system using dual-arm manipulator and high-speed fabric edge detection," *IEEE Robot. Autom. Lett.*, vol. 10, no. 9, pp. 8962–8969, 2025.
- [2] P. Taylor and D. Pollet, "Why is automated garment manufacture so difficult?" in 1997 8th International Conference on Advanced Robotics. Proceedings. ICAR'97. IEEE, 1997, pp. 39–44.
- [3] T. Gries and V. Lutz, "8 application of robotics in garment manufacturing," in *Automation in Garment Manufacturing*, ser. The Textile Institute Book Series. Woodhead Publishing, 2018, pp. 179–197.

- [4] M. Shetab-Bushehri, M. Aranda, Y. Mezouar, and E. Özgür, "Lattice-based shape tracking and servoing of elastic objects," *IEEE Trans. Robot.*, vol. 40, pp. 364–381, 2023.
- [5] H. Yin, A. Varava, and D. Kragic, "Modeling, learning, perception, and control methods for deformable object manipulation," *Sci. Robot.*, vol. 6, no. 54, p. eabd8803, 2021.
- [6] F. Tokuda, A. Seino, A. Kobayashi, K. Tang, and K. Kosuge, "Transformer driven visual servoing for fabric texture matching using dual-arm manipulator," *TechRxiv*, August 2025.
- [7] D. Seita, A. Ganapathi, R. Hoque, M. Hwang, E. Cen, A. K. Tanwani, A. Balakrishna, B. Thananjeyan, J. Ichnowski, N. Jamali, K. Yamane, S. Iba, J. Canny, and K. Goldberg, "Deep imitation learning of sequential fabric smoothing from an algorithmic supervisor," in *Proc. IEEE/RSJ Int. Conf. Intell. Robots. Syst.*, 2020, pp. 9651–9658.
- [8] K. Black, N. Brown, D. Driess, A. Esmail, M. Equi, C. Finn, N. Fusai, L. Groom, K. Hausman, B. Ichter *et al.*, "π₀: A vision-language-action flow model for general robot control," *arXiv preprint arXiv:2410.24164*, 2024.
- [9] T. Z. Zhao, V. Kumar, S. Levine, and C. Finn, "Learning fine-grained bimanual manipulation with low-cost hardware," arXiv preprint arXiv:2304.13705, 2023.
- [10] T. Z. Zhao, J. Tompson, D. Driess, P. Florence, K. Ghasemipour, C. Finn, and A. Wahid, "Aloha unleashed: A simple recipe for robot dexterity," arXiv preprint arXiv:2410.13126, 2024.
- [11] Y. Ze, G. Zhang, K. Zhang, C. Hu, M. Wang, and H. Xu, "3d diffusion policy: Generalizable visuomotor policy learning via simple 3d representations," in *Proc. Robotics Sci. Syst.*, 2024.
- [12] W. Wang, G. Li, M. Zamora, and S. Coros, "Trtm: Template-based reconstruction and target-oriented manipulation of crumpled cloths," in *Proc. IEEE Int. Conf. Robot. Autom.* IEEE, 2024, pp. 12522– 12528.
- [13] F. Tokuda, A. Seino, A. Kobayashi, and K. Kosuge, "Cnn-based visual servoing for simultaneous positioning and flattening of soft fabric parts," in *Proc. IEEE Int. Conf. Robot. Autom.* IEEE, 2023, pp. 748–754.
- [14] K. Tang, F. Tokuda, A. Seino, A. Kobayashi, N. C. Tien, and K. Kosuge, "Time-scaling modeling and control of robotic sewing system," *IEEE/ASME Trans. Mechatron.*, vol. 29, no. 4, pp. 3166– 3174, 2024.
- [15] W. Yan, A. Vangipuram, P. Abbeel, and L. Pinto, "Learning predictive representations for deformable objects using contrastive estimation," *CoRR*, vol. abs/2003.05436, 2020.
- [16] T. Tang and M. Tomizuka, "Track deformable objects from point clouds with structure preserved registration," *Int. J. Robot. Res.*, vol. 41, no. 6, pp. 599–614, 2022.
- [17] X. Lin, Y. Wang, and D. Held, "Learning visible connectivity dynamics for cloth smoothing," in *CoRL*, 2021.
- [18] Z. Huang, X. Lin, and D. Held, "Self-supervised cloth reconstruction via action-conditioned cloth tracking," arXiv preprint arXiv:2302.09502, 2023.
- [19] C. Wen, X. Lin, J. So, K. Chen, Q. Dou, Y. Gao, and P. Abbeel, "Any-point trajectory modeling for policy learning," arXiv preprint arXiv:2401.00025, 2023.
- [20] J. Hietala, D. Blanco-Mulero, G. Alcan, and V. Kyrki, "Learning visual feedback control for dynamic cloth folding," in *Proc. IEEE/RSJ Int. Conf. Intell. Robots. Syst.* IEEE, 2022, pp. 1455–1462.
- [21] E. Lo, X. Huang, K. Tang, A. Seino, F. Tokuda, and K. Kosuge, "Fabric flattening and alignment system using real-time mesh-based state estimation and visual servoing," in *Proc. IEEE Int. Conf. Mechatron. Autom.*, 2025, pp. 328–334.
- [22] Blender Online Community, "Blender a 3d modelling and rendering package," https://www.blender.org, Amsterdam, 2025, [Online; accessed September 4, 2025].
- [23] N. Ravi, J. Reizenstein, D. Novotny, T. Gordon, W.-Y. Lo, J. Johnson, and G. Gkioxari, "Accelerating 3d deep learning with pytorch3d," arXiv preprint arXiv:2007.08501, 2020.
- [24] P. Veličković, G. Cucurull, A. Casanova, A. Romero, P. Liò, and Y. Bengio, "Graph attention networks," arXiv preprint arXiv:1710.10903, 2018.
- [25] N. Ravi, V. Gabeur, Y.-T. Hu, R. Hu, C. Ryali, T. Ma, H. Khedr, R. Rädle, C. Rolland, L. Gustafson, E. Mintun, J. Pan, K. V. Alwala, N. Carion, C.-Y. Wu, R. Girshick, P. Dollár, and C. Feichtenhofer, "Sam 2: Segment anything in images and videos," arXiv preprint arXiv:2408.00714, 2024.

- [26] P. Cignoni, M. Callieri, M. Corsini, M. Dellepiane, F. Ganovelli, and G. Ranzuglia, "MeshLab: an Open-Source Mesh Processing Tool," in Eurographics Italian Chapter Conference, V. Scarano, R. D. Chiara, and U. Erra, Eds. The Eurographics Association, 2008.
 [27] R. Cadene, S. Alibert, A. Soare, Q. Gallouedec, A. Zouitine, S. Palma, P. Kooijmans, M. Aractingi, M. Shukor, D. Aubakirova, M. Russi, E. Cadene, S. Palan, P. Kooijmans, M. Aractingi, M. Shukor, D. Aubakirova, M. Russi, E. Cadene, S. Paland, P. Kooijmans, M. Aractingi, M. Shukor, D. Aubakirova, M. Russi, E. Cadene, S. Paland, P. Kooijmans, M. Aractingi, M. Shukor, D. Aubakirova, M. Russi, E. Cadene, S. Paland, P. Kooijmans, M. Shukor, D. Shukor, D.
- [27] R. Cadene, S. Alibert, A. Soare, Q. Gallouedec, A. Zouitine, S. Palma, P. Kooijmans, M. Aractingi, M. Shukor, D. Aubakirova, M. Russi, F. Capuano, C. Pascal, J. Choghari, J. Moss, and T. Wolf, "Lerobot: State-of-the-art machine learning for real-world robotics in pytorch," https://github.com/huggingface/lerobot, 2024.